



Effect and Progress of the Amorphization Process for Microscale Silicon Particles under Partial Lithiation as Active Material in Lithium-Ion Batteries

Maximilian Graf,^{1,*} Clara Berg,¹ Rebecca Bernhard,² Stefan Haufe,^{2,**} Jürgen Pfeiffer,² and Hubert A. Gasteiger^{1,**}

¹Chair of Technical Electrochemistry, Department of Chemistry and Catalysis Research Center, Technical University of Munich, Munich, Germany

²Wacker Chemie AG, Consortium für Elektrochemische Industrie, Munich Germany

Microscale silicon particles in lithium-ion battery anodes undergo large volume changes during (de)lithiation, resulting in particle pulverization and surface area increase concomitant with a continuous growth of the solid-electrolyte-interphase. One approach to overcome these phenomena is to operate the silicon anode under capacity-limited conditions (i.e., with partial capacity utilization). Since crystalline silicon is irreversibly transformed into amorphous phases upon lithiation, the purpose of the partial capacity utilization is to maintain a crystalline phase and thus prevent particle disintegration. Here, we investigate the amorphization process of micro-sized silicon particles in a silicon-rich anode (70 wt% silicon) over extended charge/discharge cycling in half-cells with a lithium reference electrode, varying the lower cutoff potential of the Si electrode. While the capacity of Si electrodes after formation remain constant for lithiation cutoffs of ≥ 170 mV vs Li^+/Li , their capacity continuously increases over cycling for cutoffs of < 170 mV vs Li^+/Li , implying an ongoing amorphization of the crystalline phase. To quantify the ratio of the amorphous phase fraction over cycling, we employed an in-situ XRD method, utilizing the copper reflex of the current collector as internal standard. This allowed to determine the extent of amorphization over the course of cycling depending on the lithiation potentials. © 2022 The Author(s). Published on behalf of The Electrochemical Society by IOP Publishing Limited. This is an open access article distributed under the terms of the Creative Commons Attribution Non-Commercial No Derivatives 4.0 License (CC BY-NC-ND, <http://creativecommons.org/licenses/by-nc-nd/4.0/>), which permits non-commercial reuse, distribution, and reproduction in any medium, provided the original work is not changed in any way and is properly cited. For permission for commercial reuse, please email: permissions@iopublishing.org. [DOI: [10.1149/1945-7111/ac4b80](https://doi.org/10.1149/1945-7111/ac4b80)]



Manuscript submitted October 27, 2021; revised manuscript received December 13, 2021. Published February 11, 2022. This was Paper 357 presented during PRiME 2020, October 4–9, 2020.

With a specific electrochemical capacity of $3579 \text{ mAh g}_{\text{Si}}^{-1}$, silicon is a promising candidate for next generation Li-ion batteries, as it exceeds the capacity of commonly used graphite by a factor of 10.^{1,2} However, large volume changes upon (de-)alloying up to $\sim 300\%$ lead to mechanical stress in the active material resulting in particle pulverization.^{1,3} This causes the loss of electrical contact and excessive electrolyte reduction; the resulting excessive solid-electrolyte-interphase (SEI) formation still hampers a broad application of silicon as anode material up to now.^{2,4–6} In the past, several strategies have been proposed to reduce the effect of the volume expansion. Among them, nanostructured silicon has shown to sustain the stress and reduce the degradation phenomena mentioned above.⁷ The large surface area of pristine nanostructured silicon however is connected to significant SEI formation and therefore large irreversible lithium losses in the formation process.^{6,8} In addition, large-scale production of nanostructured material designs remains difficult and expensive.

To compete against current graphite systems, the production of silicon material needs to be scalable and cost-effective. Microscale silicon particles which meet these requirements are therefore still in the focus of research. To overcome the aforementioned issues, innovative binder systems such as self-healing^{9,10} or highly elastic polymers,¹¹ which can reduce the impact of the volume expansion for μm -sized particles, have been developed. Another promising concept is to use only a part of the total silicon capacity available and therefore reduce the volume expansion upon (de)lithiation, as demonstrated for both Si nanowires¹² and μm -sized silicon particles.^{13–16} Some of these studies showed that limiting the utilized silicon anode capacity to $1200 \text{ mAh g}_{\text{Si}}^{-1}$ (corresponding to $\sim 30\%$ of the theoretical capacity of Si) can improve the cycling stability and significantly reduces pulverization even of μm -sized Si particles.^{13,15,16} Next to the limited volume expansion with this approach, another advantage is to prevent formation of the crystalline $\text{Li}_{3.75}\text{Si}$ phase at low voltages, which is associated with a large

overpotential during delithiation.¹⁷ The degree of utilization of silicon in full-cells can be controlled by the balancing of anode and cathode areal capacity, such that upon initial charging only a limited amount of silicon is converted to the amorphous phase, in which case a significant fraction of crystalline silicon could in principle be retained during cycling. As TEM measurements have shown that repeated (de)lithiation of only the amorphous phase results in isotropic expansion that is less prone to lead to particle cracking, whereas the anisotropic expansion of crystalline silicon leads to tensile stress and cracking,¹⁸ retaining a crystalline phase in partially (de)lithiated silicon would be expected to be beneficial. Contrary to a fully amorphous Si particle where the restriction of the capacity would lead to a higher average anode voltage (i.e., to a lower achievable energy density), the crystalline phase in this approach acts as inactive phase.² Therefore, the phase composition of the lithiated Si-phase is richer in lithium compared to the case when the silicon particle is completely amorphous, and thus has a lower average anode voltage (i.e. to a higher achievable energy density). That partially lithiated μm -sized silicon particles would be able to retain a crystalline cores was deduced by Obrovac et al.³ using electrochemical methods, suggesting that the crystalline silicon phase would be preserved for lithiation potentials of ≥ 170 mV vs Li^+/Li , where only the amorphous silicon phase is being lithiated. However, this conclusion was not confirmed by a direct quantification of the remaining crystalline phase over the course of extended charge/discharge cycling. Therefore, in this study, we present an in-situ XRD method to track the crystalline phase fraction of partially lithiated μm -sized silicon particles, investigating different lithiation potentials during cycling in relation to the amorphization progress of the remaining crystalline silicon. Furthermore, the degradation of the here used microscale silicon particles caused by progressive amorphization is analyzed, and implications on their cycle-life are discussed.

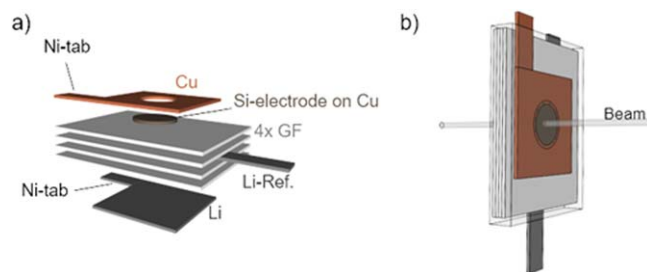
Experimental

Electrode preparation.—Silicon electrodes with graphite as conductive agent were prepared by suspending 7.0 g Si-powder (BET: 1.6

*Electrochemical Society Student Member.

**Electrochemical Society Fellow.

^zE-mail: Maximilian.graf@tum.de



Scheme 1. Setup of the Si//Li pouch-cells for in-situ XRD measurements, (a) The cell is composed of a Li-metal ($450\ \mu\text{m}$ thick, $30 \times 30\ \text{mm}^2$, 99.9%, Rockwood Lithium, USA) counter electrode (plotted at the bottom), 4 glassfiber separators (Whatman GD type A/E, $45 \times 55\ \text{mm}^2$, USA), and a Si-KS6L working electrode (11 mm diameter) coated on a thin copper foil (11 μm). To connect the Si-KS6L working electrode with the Ni-tab, an additional copper foil was used (plotted at the top), containing a hole (10 mm diameter) that is slightly smaller than the size of the Si-KS6L electrode in order to allow for good electronic connection without reducing the X-ray beam intensity. The Li-reference, a Li-metal piece connected to a Ni-tab, was placed in between the glassfiber separators. (b) Configuration of the assembled cell, marking the position of the X-ray beam.

$\text{m}^2\ \text{g}^{-1}$, $d_{10} = 2.2\ \mu\text{m}$, $d_{50} = 4.5\ \mu\text{m}$, $d_{90} = 7.8\ \mu\text{m}$; CLM 00001, Wacker Chemie AG) in 5.1 g H_2O and 12.5 g of an LiPAA solution (4 wt%) in a dissolver mixer (Dispermat LC30, VMA-Getzmann). The LiPAA solution was prepared by neutralization of PAA solution (polyacrylic acid, $M_v = 459\ \text{k}$, Sigma Aldrich) with lithium hydroxide (LiOH, Sigma Aldrich) to a pH of 7. In the next step, 2.5 g graphite (KS6L, Imerys) was added to yield a mass ratio of 70:25:5 Si/KS6L/LiPAA and stirring was continued at 12000 rpm for 30 min.

In addition, silicon model electrodes with carbon black (Super C65, Timcal) as conductive additive were examined, as they allow for a more rigorous analysis of the charge/discharge features of silicon due to the absence of the graphite-derived features in the electrodes with the KS6L graphite. For this, a suspension of 8.5 g Si-powder (CLM 00001, Wacker Chemie AG) in 20.0 g H_2O and 12.5 g of a LiPAA solution (4 wt%) was prepared in a dissolver mixer. Then, 1.0 g Super C65 was added and mixed for $3 \times 5\ \text{min}$ at 2000 rpm in a planetary mixer (Thinky Corp., USA), yielding a mass ratio of 85:10:5 Si/C65/LiPAA.

For degassing, the slurries were mixed at 2000 rpm for 5 min in a planetary mixer (Thinky Corp., USA). The slurries were coated onto a copper foil (15 μm) with a box-type coating bar (Erichsen, Hemer, Germany) using an automated coater (RK PrintCoat Instruments, UK), and dried at room temperature overnight. Electrodes with a diameter of 11.0 mm were punched out from the above prepared electrode coatings. After drying at 120 C under vacuum over night, the Si electrode coatings with graphite as conductive agent had a loading of $2.1\ \text{mg}_{\text{Si}}\ \text{cm}^{-2}$ ($\equiv 7.5\ \text{mAh}\ \text{cm}^{-2}$ based on $3579\ \text{mAh}\ \text{g}_{\text{Si}}^{-1}$) and a thickness of $\sim 34\ \mu\text{m}$, and will in the following be referred to as “Si-KS6L” electrodes. The electrodes with C65 as conductive additive had a loading of $1.4\ \text{mg}_{\text{Si}}\ \text{cm}^{-2}$ ($\equiv 5.0\ \text{mAh}\ \text{cm}^{-2}$ based on $3579\ \text{mAh}\ \text{g}_{\text{Si}}^{-1}$) and a thickness of $\sim 17\ \mu\text{m}$, and will in the following be referred to as “Si-C65.” All electrodes were then transferred to an argon-filled glove box ($< 1\ \text{ppm}\ \text{O}_2$ and H_2O , MBraun, Germany) without exposure to air.

Cell-assembly.—Differential capacity analysis of the Si-C65 electrodes was conducted in half-cells using a spring-compressed Swagelok® T-cell setup with a metallic lithium reference electrode (RE). The cells were assembled with two glass fiber separators (Whatman GD type A/E, USA) and $90\ \mu\text{l}$ 1M LiPF_6 in FEC:DEC 2:8 v/v ($< 20\ \text{ppm}\ \text{H}_2\text{O}$; Gelon, China) against metallic lithium (450 μm thick, 11 mm diameter, 99.9%, Rockwood Lithium, USA). Investigations on the cycling behavior with different lithiation cutoff potentials were conducted with Si-KS6L electrodes containing graphite as conductive agent, using the same cell setup.

In situ XRD experiments were performed on Si//Li pouch cells with a metallic lithium RE, using a thin pouch foil (12 μm thick Al layer) in order to reduce the attenuation of the X-ray beam and the intensity of the Al-derived diffraction peaks. Si-KS6L anodes with 11 mm diameter were assembled vs a lithium counter electrode (450 μm thick, $30 \times 30\ \text{mm}^2$, 99.9%, Rockwood Lithium, USA) with four glass fiber separators (Whatman GD type A/E, $45 \times 55\ \text{mm}^2$, USA) in 2000 μl 1M LiPF_6 in FEC:DEC 2:8 v/v ($< 20\ \text{ppm}\ \text{H}_2\text{O}$; (Gelon, China). A piece of lithium ($10 \times 5\ \text{mm}^2$) connected to a Ni-tab which was positioned between the separators was used as reference electrode. A sketch of the pouch cell configuration is shown in Scheme 1. To avoid the formation of mossy lithium on the Li-counter electrode, the cells were cycled in a homemade spring-loaded pouch cell holder with a compression of $\sim 25\ \text{bar}$. For in-situ XRD measurements, cell-cycling was stopped after delithiation to 1.5 V vs Li^+/Li , the pouch cell was removed from the spring-loaded holder and placed into a custom made XRD holder.

Cell testing.—All electrochemical cycling tests were performed in a climate chamber (Binder, Germany) at 25 °C, using a multi-channel potentiostat (Biologic VMP3).

To investigate the silicon phase transition in the dQ/dV plot, the Si-C65 model electrodes were initially lithiated to a specific capacity of $1500\ \text{mAh}\ \text{g}_{\text{Si}}^{-1}$ with constant current cycling at a rate of C/25 (based on $3579\ \text{mAh}\ \text{g}_{\text{Si}}^{-1}$), followed by delithiation to a cutoff potential of 1.5 V vs the lithium reference electrode. For the second cycle, the electrodes were cycled with a rate of C/25, in one case to the same specific capacity limit of $1500\ \text{mAh}\ \text{g}_{\text{Si}}^{-1}$, and in the other case to the lithiation cutoff potential of 170 mV vs Li^+/Li followed by delithiation to 1.5 V vs Li^+/Li .

To study the effect of varying lower lithiation cutoffs on the cycling behavior, the Si-KS6L silicon electrodes (70:25:5 Si/KS6L/LiPAA) were lithiated at a constant current rate of C/60 (based on $3579\ \text{mAh}\ \text{g}_{\text{Si}}^{-1}$) in the first cycle to a specific capacity limit of $600\ \text{mAh}\ \text{g}_{\text{Si}}^{-1}$ for one set of cells and to $1500\ \text{mAh}\ \text{g}_{\text{Si}}^{-1}$; the cells were then delithiated at C/60 until a cutoff of 1.5 V vs Li^+/Li . Subsequent cycling was conducted at C/60 to different lithiation cutoff potentials set in the range of 140–180 mV vs Li^+/Li with a CV step at the end of lithiation until a current of C/120; delithiation was again performed at C/60 until a cutoff of 1.5 V vs Li^+/Li . In order to ensure comparability between the capacity limit of $600\ \text{mAh}\ \text{g}_{\text{Si}}^{-1}$ and $1500\ \text{mAh}\ \text{g}_{\text{Si}}^{-1}$, the same absolute current densities are applied and therefore referred to the maximum theoretical capacity of $3597\ \text{mAh}\ \text{g}_{\text{Si}}^{-1}$ for clarification (i.e. C/60 corresponds to C/10 and C/25 when referred to the actual capacity usage of $600\ \text{mAh}\ \text{g}_{\text{Si}}^{-1}$ and $1500\ \text{mAh}\ \text{g}_{\text{Si}}^{-1}$ respectively).

For the in situ XRD experiments, Si-KS6L silicon electrodes were lithiated to either $600\ \text{mAh}\ \text{g}_{\text{Si}}^{-1}$ or $1500\ \text{mAh}\ \text{g}_{\text{Si}}^{-1}$ at C/60 (based on $3579\ \text{mAh}\ \text{g}_{\text{Si}}^{-1}$), followed by delithiation to 1.5 V vs Li^+/Li at C/60. Consecutive cycles of cells with the different first-cycle capacity limits were lithiated to either 170 mV vs Li^+/Li or 140 mV vs Li^+/Li with a rate of C/30 and a CV step at the end of lithiation until a current of C/120. Prior to the in-situ XRD measurements, the cells were put into open circuit voltage (OCV) hold at the end of selected lithiation cycles.

X-ray powder diffraction measurements.—The in-situ XRD study on the Si//Li pouch cells was performed using a STOE STADI P diffractometer (STOE & Cie GmbH, Darmstadt, Germany) in transmission mode using $\text{Mo-K}_{\alpha 1}$ radiation (0.7093 Å, 50 kV, 40 mA) and a Mythen 1 K detector. For this, a cycled pouch cell was transferred from the spring-loaded pouch cell holder to a homemade holder for mounting the pouch cell to the diffractometer, equipped with 15 mm diameter holes in the holder fixture to give access to the X-ray beam (for details see reference Strehle et al.¹⁹). Data collection was performed after delithiating the cells to 1.5 V vs Li^+/Li and comprise the pristine cell (i.e. assembled cell before electrochemical testing), after cycle 1, cycle 11, cycle 21, cycle 31

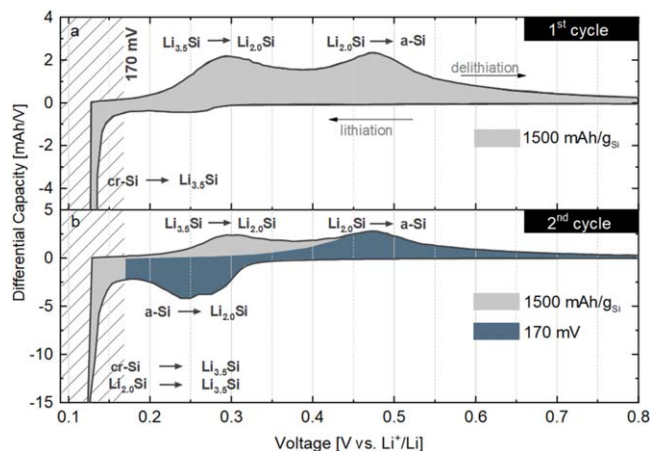


Figure 1. Differential capacity vs Li-Re curves obtained from constant current cycling ($C/25$, referenced to $3579 \text{ mAh g}_{\text{Si}}^{-1}$) of Si-C65/Li ($1.4 \text{ mg}_{\text{Si}} \text{ cm}^{-2}$, with a theoretical capacity of 5.0 mAh cm^{-2}) Swagelok® T-cells with a Li-RE: (a) First cycle where, the lithiation step was limited to $1500 \text{ mAh g}_{\text{Si}}^{-1}$, followed by consecutive delithiation to a cutoff potential of 1.5 V vs Li^+/Li measured against the Li-RE. (b) Second cycle, where the lithiation was limited either by a capacity cutoff of $1500 \text{ mAh g}_{\text{Si}}^{-1}$ (gray area) or by a voltage cutoff of 170 mV vs Li^+/Li (blue area). Electrochemical testing was done at 25°C with 1M LiPF_6 in FEC/DEC (2:8 v-v) and with two glassfiber separators.

and cycle 41. Measurements were conducted over night ($\sim 14 \text{ h}$) in a 2θ range of $12.5\text{--}39^\circ$ with detector step size/step time of $0.06^\circ/45 \text{ s}$.

The diffraction data were reduced with the software WinXPOW (V3.0.2.1, STOE & Cie GmbH, Darmstadt, Germany 2011) and refined with the software package Topas (TOPAS-Academic V6, Coelho Software, Brisbane, Australia 2016). Rietveld refinement was conducted for the silicon and copper phase using the Thompson-Cox-Hastings pseudo-Voigt function (TCHZ) to describe the peak profiles. The refinements included the following non-structural parameters:

- background: Chebyshev polynomial with 1β parameters
- instrument: zero shift and axial divergence

The structure-related refinement parameters are the following:

- Cu (225, $Fm\bar{3}m$)
 - a. Lattice parameter a_{Cu} ($=3.61 \text{ \AA}$)
 - b. Atomic displacement parameter b_{Cu} ($=1.2 \text{ \AA}$)
 - c. TCHZ peak parameters V_{Cu} , Z_{Cu} , Y_{Cu} are fixed to (0/0/0)
 - d. TCHZ peak parameters U_{Cu} , W_{Cu} , X_{Cu} are refined
- Si (227, $Fd\bar{3}m$)
 - a. Lattice parameter a_{Si} ($=5.40\text{--}5.44 \text{ \AA}$)
 - b. Atomic displacement parameter b_{Si} is fixed to 0.5 \AA
 - c. TCHZ peak parameters V_{Cu} , Z_{Cu} , Y_{Cu} are fixed to (0/0/0)
 - d. TCHZ peak parameters U_{Cu} , W_{Cu} , X_{Cu} are refined

SEM cross-sections.—Sample preparation and post-mortem SEM cross-sections were made at WACKER Chemie AG using a scanning electron microscope (Ultra 55 from Carl Zeiss Microscopy, Germany) with a thermal field emission cathode. The electrode samples were harvested from the cells, rinsed with 3 ml DMC in order to remove remaining conductive salt and dried for 12 h at RT under vacuum. After this, the electrodes were prepared for analysis in an argon filled glove box, and then transferred under inert atmosphere into an IonMill 4000 Plus (Hitachi High Technologies; 6 kV ion beam slope cutting). Via a specimen transfer module (Kammrath & Weiss), samples were transferred under argon atmosphere from the glove box to the measuring chamber of the SEM. Magnifications between $30 \times$ and $30,000 \times$ were chosen using the SE-mode (secondary electrons) at high vacuum ($\sim 10^{-6} \text{ mbar}$) with an energy of the electron beam of 3 kV .

Results and Discussion

Effect of lithiation capacity and potential cutoff on electrochemical behavior.

—In the following, the lithiation and delithiation behavior of silicon and its phase transitions at different potentials is investigated with the Si-C65 model electrodes containing 85% silicon and 10% C65 as conductive agent, Fig. 1 shows the differential capacity (dQ/dV) plot of the first cycle of a Si-C65||Li Swagelok® T-cell with a Li-RE. In the pristine state, the silicon is present in its crystalline phase. Upon its initial lithiation, the alloying reaction of crystalline silicon with lithium takes place at a potential $< 170 \text{ mV}$ vs Li^+/Li , marked by the dashed area in the dQ/dV -plot shown in Fig. 1, leading to the formation of amorphous Li_xSi phase. The lithiation potential of crystalline silicon is often reported to be lower than 170 mV ,^{20,21} as this progress is kinetically hindered and therefore can lead to large polarizations depending on the applied current rate.³ At very low currents, Limthongkul et al. reported that the first lithiation of crystalline silicon occurred at $\sim 180 \text{ mV}$ vs Li^+/Li .²² In Fig. 1, the lithiation step is terminated at a specific capacity of $1500 \text{ mAh g}_{\text{Si}}^{-1}$ that corresponds to 42% of the total theoretical capacity of $3579 \text{ mAh g}_{\text{Si}}^{-1}$ (the maximum for the highest lithiated phase of $\text{Li}_{3.75}\text{Si}$), so that one would expect a significant fraction of the silicon particles to remain in their crystalline phase. During delithiation two distinct phase transition features can be observed in Fig. 1a between $200\text{--}400 \text{ mV}$ and $400\text{--}600 \text{ mV}$ vs Li^+/Li : the former can be ascribed to the delithiation of a higher lithiated phase ($\text{Li}_{3.5}\text{Si}$) to a lower lithiated phase ($\text{Li}_{2.0}\text{Si}$), the latter to the consecutive delithiation of the lower lithiated phase to a fully delithiated amorphous Si phase.^{20,23–26} The presence of two delithiation features during the first delithiation implies that a highly lithiated phase ($\text{Li}_{3.5}\text{Si}$) is readily formed once the potential is reached where alloying of crystalline silicon is possible. This was also shown in solid-state NMR studies, where the amorphous phase formed upon lithiating the crystalline phase is highly lithiated, with an average composition of the Li_xSi phase corresponding to $x = 3.4 \pm 0.2$.²¹ This is suggested to be due to the required large activation energy and therefore high concentration of Li atoms to break the Si-Si bonds in the crystalline phase.^{18,27,28} Therefore, it is kinetically more favorable to first break the remaining Si-Si bonds within the amorphous phase before lithiating the unreacted crystalline Si framework.²⁹

When limiting the subsequent second lithiation cycle again to a capacity of $1500 \text{ mAh g}_{\text{Si}}^{-1}$, as marked by the sum of the gray and blue area in Fig. 1b, the onset of a lithiation feature is now already observed at potentials below $\sim 350 \text{ mV}$, which has been ascribed to the alloying reaction of the amorphous Si phase and lithium to form the lower lithiated phase with a composition of $\text{Li}_{2.0}\text{Si}$.^{20,26} At potentials below 170 mV , a second feature similar to the one observed in the first cycle appears, corresponding to the further lithiation of crystalline silicon. During the subsequent delithiation, two features are observed again, confirming the formation of the $\text{Li}_{3.5}\text{Si}$ also in the second cycle when the second-cycle lithiation is terminated at the same capacity as for the first cycle (i.e., at $1500 \text{ mAh g}_{\text{Si}}^{-1}$). On the other hand, if the second lithiation cycle terminated at 170 mV , i.e., prior to the second lithiation feature (marked by the blue area in Fig. 1b), the higher lithiated $\text{Li}_{3.5}\text{Si}$ phase is not formed, and thus only the delithiation feature of the $\text{Li}_{2.0}\text{Si}$ phase is observed, which is in line with the findings of a former study.³⁰ In summary, for the capacity-limited lithiation the alloying reaction of crystalline silicon takes place also in the second cycle, implying that further amorphization of the crystalline Si phase is possible in the case of capacity limited cycling even in the second cycle. However, when terminating the second lithiation cycle at a cutoff of 170 mV , the formation of the lithium-rich $\text{Li}_{3.5}\text{Si}$ phase and thus the amorphization of the remaining crystalline silicon are prevented. In the following, varying lithiation potential cutoff limits are examined and their effect on the retention of the crystalline Si phase are discussed.

To determine the lower cutoff potential at which continuous amorphization of the crystalline silicon occurs upon cycling, Si||Li

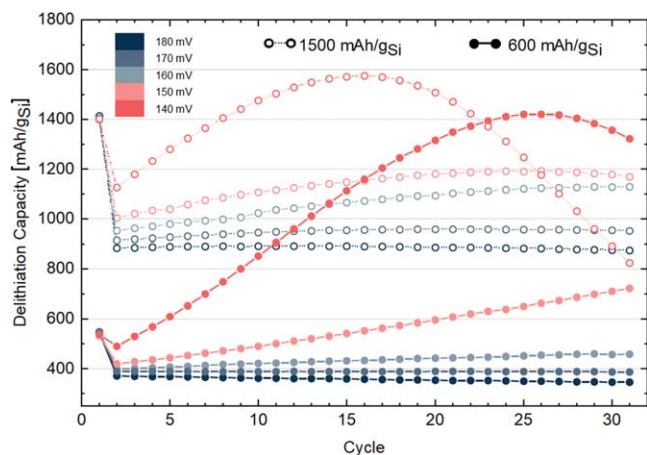


Figure 2. Delithiation capacity of Si-KS6L//Li ($2.1 \text{ mg}_{\text{Si}} \text{ cm}^{-2}$, with a theoretical capacity of 7.5 mAh cm^{-2}) Swagelok® T-cells with varying lower cutoff limits for lithiation potentials (set between 180 mV vs Li^+/Li (blue) to 140 mV vs Li^+/Li (red)). Formation cycles were conducted at C/60 (referenced to $3579 \text{ mAh g}_{\text{Si}}^{-1}$) until a specific lithiation capacity of either 600 $\text{mAh g}_{\text{Si}}^{-1}$ (solid symbols) or 1500 $\text{mAh g}_{\text{Si}}^{-1}$ (open symbols) was reached. Subsequent cycling was conducted at C/60 with a CV step at the end of lithiation until a current of C/120, while delithiation was performed at C/60 until a cutoff of 1.5 V vs Li^+/Li . Experiments were conducted at 25°C with 1M LiPF_6 in FEC/DEC (2:8 v-v) and with two glassfiber separators.

cells with a Li-RE were cycled at C/60 with different lithiation cutoff potentials between 140 mV and 180 mV vs Li^+/Li with respect to the Li-RE. To ensure a stable cycling performance, the Si-KS6L electrodes with conductive graphite additive are used instead of the Si-C65 electrodes, as the latter showed only poor cycling stability for longer cycling. It should be noted that the KS6L graphite here only acts as conductive additive, since at these high lithiation potentials the contribution of graphite to the overall electrode capacity are negligible. Figure 2 shows the cycling data for the cells limited to a specific lithiation capacity of either 600 $\text{mAh g}_{\text{Si}}^{-1}$ (solid symbols) or 1500 $\text{mAh g}_{\text{Si}}^{-1}$ (open symbols) in the first lithiation cycle, leading to different initial ratios of amorphous and crystalline phase in the first cycle.

For the cells cycled to an initial lithiation capacity of 600 $\text{mAh g}_{\text{Si}}^{-1}$, the cutoff potentials of 180 and 170 mV (dark blue and blue solid symbols in Fig. 2) show a stable cycling behavior with no capacity increase over 31 cycles. Lowering the lithiation cutoff potential to below 170 mV leads to a continuous capacity increase (light blue, light red, and red solid symbols). Therefore, the lower the cutoff potential, the more pronounced is the capacity increase over cycling, which is in good agreement with the results from Obrovac et al., who reported the same behavior for cells with μm -sized silicon particles cycled to below 170 mV.³ For the cell with the lowest cutoff potential of 140 mV (red solid symbols), the rate of capacity increase upon cycling decreases until after ~ 25 cycles the capacity starts to decrease slightly. We believe that at this point a substantial fraction of the crystalline silicon phase has been consumed, so that the mechanical integrity of silicon particles cannot be maintained anymore, leading to degradation and capacity loss. Cells initially lithiated to 1500 $\text{mAh g}_{\text{Si}}^{-1}$ also show no capacity increase for lithiation cutoff potentials of 170 and 180 mV (dark blue and blue open symbols in Fig. 2) as well as a gradual capacity increase at lower cutoff potentials. For the lowest cutoff potential of 140 mV (dark red open symbols), the rate of capacity increase again gradually declines until the capacity starts to rapidly decrease after ~ 15 cycles, analogous but more pronounced compared to what was observed for the cells lithiated to an initial capacity of 600 $\text{mAh g}_{\text{Si}}^{-1}$. This can be explained by the higher amorphous phase fraction formed when the initial lithiation capacity is higher, so that upon continuous cycling to low cutoff voltages the

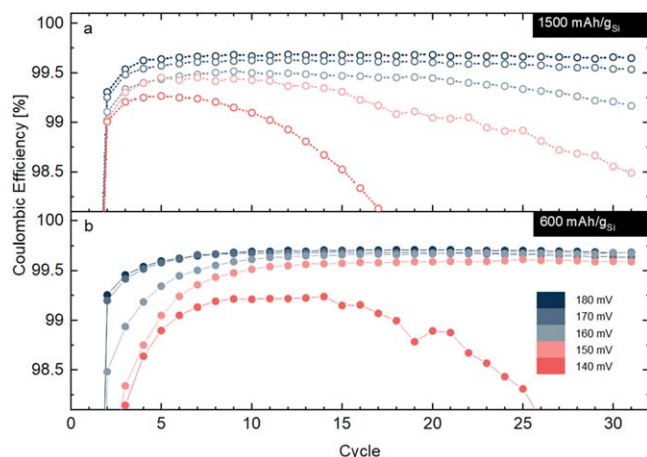


Figure 3. Coulombic-efficiency of the Si-KS6L//Li cells derived from the cycling data shown in Fig. 2 for the two different first-cycle lithiation capacities: (a) 1500 $\text{mAh g}_{\text{Si}}^{-1}$; (b) 600 $\text{mAh g}_{\text{Si}}^{-1}$. The coulombic-efficiency data is shown for varying lithiation cutoff potential limits ranging from 140–180 mV vs Li^+/Li (for further experimental details, see caption of Fig. 2).

stabilizing crystalline silicon phase gets depleted below a critical amount at a lower number of cycles.

The coulombic efficiency (CE) of the above described Si-KS6L//Li cells is shown in Fig. 3. For both of the initial lithiation capacities of 1500 $\text{mAh g}_{\text{Si}}^{-1}$ (Fig. 3a) and 600 $\text{mAh g}_{\text{Si}}^{-1}$ (Fig. 3b), cells with a cutoff lithiation potential of 180 and 170 mV reveal the highest CE (dark blue and blue symbols), exceeding 99.5% in the third cycle and beyond. On the other hand, lower lithiation cutoffs lead to a proportionally decreasing CE, particularly observed for the cells initially lithiated to 1500 $\text{mAh g}_{\text{Si}}^{-1}$. This, we believe, is due to silicon particle cracking upon depletion of the stabilizing crystalline silicon phase, leading to enhanced SEI growth and/or a loss of electronic contact of the fractured silicon particles.

To further examine the effect of the lithiation cutoff potential on the amorphization of the silicon particles, we compare the dQ/dV plots over cycling with two different lithiation cutoff potentials, namely with 170 mV and 140 mV, representing two different characteristics: for the former, the capacity remains constant over cycling, while for the latter a continuous capacity increase over cycling is observed, ultimately followed by rapid decrease of the capacity and the CE (see Figs. 2 and 3). Figure 4 depicts the dQ/dV plot of the Si-KS6L//Si cells with a cutoff of 170 mV (blue) and 140 mV (red) over the course of 31 cycles, exemplarily shown for the cells with an initial lithiation capacity of 1500 $\text{mAh g}_{\text{Si}}^{-1}$ (derived from the data shown in Fig. 2). As already observed for the Si-C65 model electrodes examined in Fig. 1, for a lithiation potential cutoff of 170 mV, only one delithiation feature representative of the delithiation of the $\text{Li}_{2.0}\text{Si}$ phase is observed, implying that the lithiation cutoff potential was too high for the formation of the $\text{Li}_{3.5}\text{Si}$ phase. In this case, the dQ/dV features remain unchanged over the course of the 31 cycles, indicating that the fraction of the amorphous phase does not increase.

On the other hand, when the lithiation potential cutoff is decreased to 140 mV (red lines), the $\text{Li}_{3.5}\text{Si}$ feature during delithiation is increasing over the course of cycling, together with the $\text{Li}_{2.0}\text{Si}$ (de)lithiation features. This continuous increase of the capacity associated with the $\text{Li}_{2.0}\text{Si}$ features can only be explained by a growth of the fraction of the amorphous phase of the silicon particles. Thus, the continuous lithiation of the crystalline silicon phase and the associated formation of an amorphous silicon phase over the course of cycling seems to occur once the $\text{Li}_{3.5}\text{Si}$ feature starts to evolve, implying that the formation of the $\text{Li}_{3.5}\text{Si}$ phase is required for the lithiation of the crystalline silicon phase. These observations support the conclusions that a high lithium

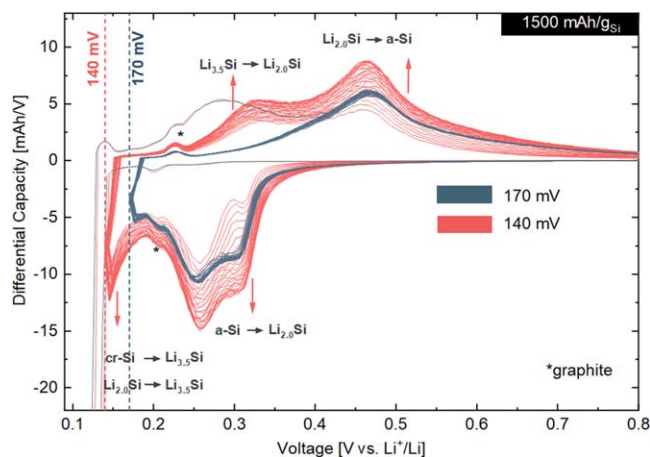


Figure 4. Differential capacity vs Li-RE curves obtained from constant current cycling (C/60, referenced to 3579 mAh g_{Si}^{-1}) of Si-KS6L//Li Swagelok® T-cells lithiated in the first cycle to 1500 mAh g_{Si}^{-1} and subsequently cycled to two different lithiation potential cutoffs: 170 mV vs Li^+/Li (blue) and 140 mV vs Li^+/Li (red); note, the lithiation potential was held until the current decayed to C/120. The delithiation was terminated by a cutoff potential of 1.5 V vs Li^+/Li measured against the Li-RE. The plot is derived from the measurements shown in Fig. 2. The asterisk marks the features due to the graphite component in the electrode.

concentration is needed to break the silicon bonds for the alloying reaction of crystalline silicon with lithium.^{18,21,27–29}

Effect of lithiation capacity and potential cutoff on the silicon particle morphology.—In the following, the effect of different cutoff potentials on the silicon particle morphology is investigated and discussed. Figure 5 shows the cross-sectional view of a pristine Si-KS6L electrode and of electrodes harvested after 31 cycles with cutoffs at 170 mV and 140 mV according to the measurements shown in Fig. 2. In the pristine electrode the silicon particles appear in bright gray and exhibit a smooth homogeneous cross sectional surface with no cracks, while the graphite flakes appear in darker gray (see upper and lower panel of Fig. 5a). For both initial lithiation capacities of 600 mAh g_{Si}^{-1} and 1500 mAh g_{Si}^{-1} , silicon particles appear in the delithiated state in bright grey and the graphite flakes in

darker grey. The Si-KS6L electrodes harvested after 31 cycles with a lithiation potential cutoff of 170 mV show some minor cracks primarily near the surface of the silicon particles (see upper and lower panels of Figs. 5b and 5c), especially for the cell cycled to 1500 mAh g_{Si}^{-1} . Independent of their initial lithiation capacities, however, the cores of the silicon particles appear to be without structures and cracks, resembling the characteristics of the pristine silicon particles.

In contrast, the silicon particles of the harvested Si-KS6L electrodes cycled with a lithiation cutoff potential of 140 mV reveal a highly structured particle cross-section throughout the whole core of the silicon particles, and only isolated segments of non-structured areas can be observed. This structuring was observed for ~50% of the silicon particles in the cross-sectional images, indicating an inhomogeneous degradation of the silicon particles. This could be explained by the polycrystalline nature of the pristine silicon material, as different crystal orientations show varying lithiation kinetics.³¹ The electrodes with 600 mAh g_{Si}^{-1} and 1500 mAh g_{Si}^{-1} harvested after 31 cycles exhibit the same extent of structured areas, which is consistent with the cycling data shown in Fig. 2: while the capacity gain of the cell with 600 mAh g_{Si}^{-1} and a lithiation cutoff potential of 140 mV is larger compared to the one with 1500 mAh g_{Si}^{-1} , the maximum capacity reached is almost the same for both electrodes, suggesting similar extents of particle fracturing. In summary, the cross-sectional views of the silicon particles of the cycled electrodes display a significant degradation of the silicon particles for cells cycled to a lithiation cutoff potential of 140 mV, while no pronounced morphological changes of the silicon particles are observed when the lithiation cutoff potential is restricted to 170 mV.

XRD analysis on the effect of lithiation capacity and potential cutoff.—To further understand and validate the conclusions with regards to the amorphization of the silicon particles upon cycling that were drawn from the analysis of the dQ/dV and the cycling experiments with different lithiation cutoff potentials, we now want to follow the cycling-induced amorphization process of the Si particles by quantifying the amount of the crystalline silicon phase in the pristine and cycled electrodes. For this, in-situ X-ray diffraction (XRD) data were acquired from Si-KS6L/Li pouch cells with a Li-RE, whereby the cells were cycled according to the cycling procedure shown in Fig. 2. The cells were cycled in a pouch cell

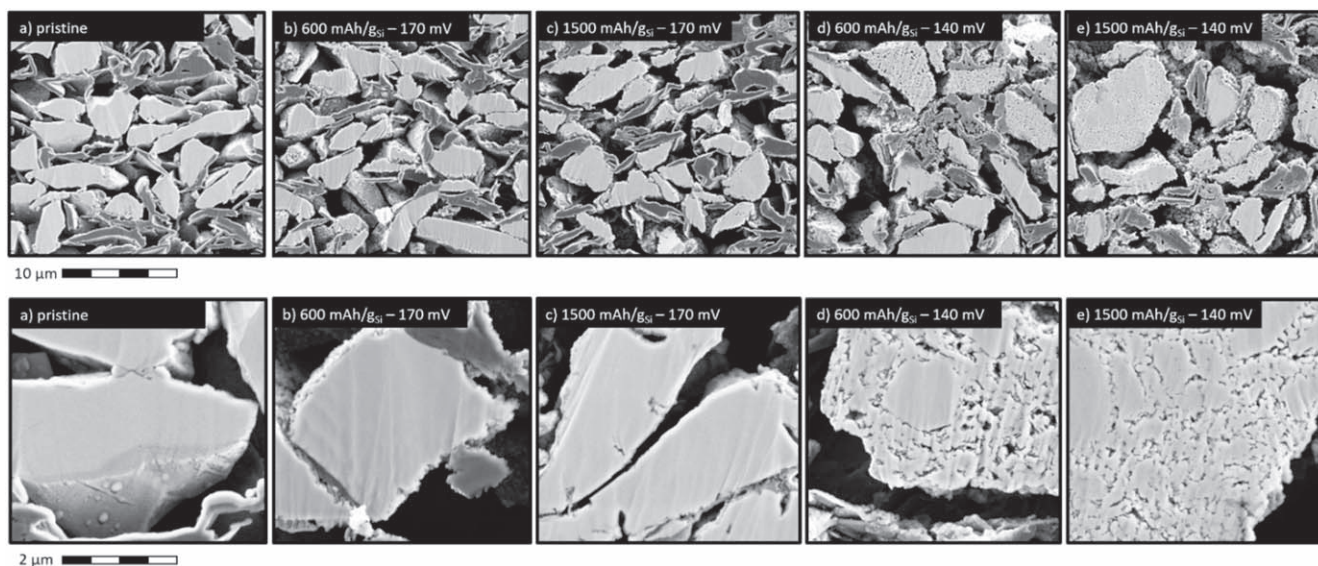


Figure 5. Effect of different lithiation cutoff potentials on the silicon particle morphology based on cross-sectional SEM images (secondary electron mode at 3 kV) of Si-KS6L electrodes in their pristine state or harvested after 31 cycles: (a) pristine electrode; (b) initial lithiation of 600 mAh g_{Si}^{-1} and cycling with a lithiation cutoff potential of 170 mV; (c) initial lithiation of 1500 mAh g_{Si}^{-1} and cycling to 170 mV; (d) initial lithiation of 600 mAh g_{Si}^{-1} and cycling to 140 mV; (e) initial lithiation of 1500 mAh g_{Si}^{-1} and cycling to 140 mV.

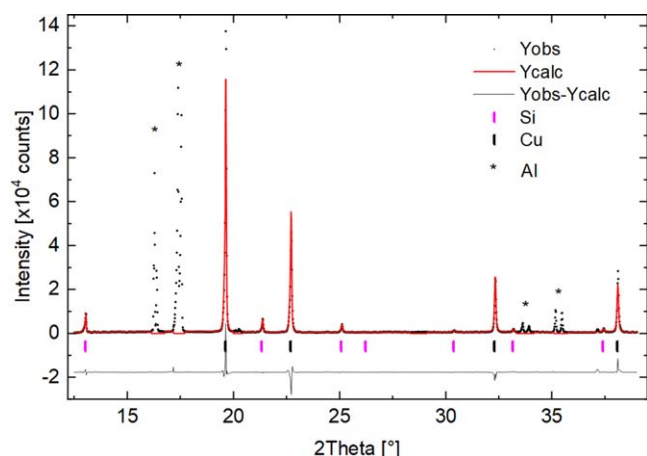


Figure 6. In situ XRD data (black data points) obtained from a pristine Si-KS6L/Li-pouch cell, including a Rietveld refinement fit (red line) and the difference plot (thin black line). Data were collected on an in-house diffractometer in transmission mode using Mo-K α_1 radiation. The vertical ticks mark the Bragg peaks of silicon (magenta) in the electrode and of copper (black) from the anode current collector; the asterisks mark the aluminum reflections from the pouch foil. Note that for the refinement only silicon and copper reflections are considered, i.e., the regions near the aluminum peaks were omitted from the fit.

holder (compressed at ~ 25 bar) and then, either after the first formation cycle (cycle #1) or after sets of 10 cycles (i.e., cycle #11, #21, etc.), they were transferred in their delithiated state to the XRD sample holder for XRD analysis. For the quantification, the cell was also analyzed in the pristine state and the data are reported as cycle #0. To ensure the very same beam position at the electrode within one measurement series of a cell, the exact position of the pouch cell in the XRD holder was marked on the pouch foil on each cell.

Figure 6 shows the diffraction pattern (black dots) of a pristine Si-KS6L/Li pouch cell, where next to the diffraction peaks of crystalline silicon (reflections marked by the magenta ticks), one can observe the copper diffraction peaks from the silicon anode current collector (marked by the black ticks) and the aluminum diffraction peaks from the pouch foil (marked by asterisks). To quantify the amount of crystalline silicon that is being retained over cycling, the silicon diffraction intensity of cells after formation or after cycling is

analyzed and referenced to the silicon diffraction intensity obtained with the pristine cell. In order to account for absolute changes of the intensities between each measurement due to small variations of the incident beam intensity, the silicon reflex intensity was referenced to an internal standard. For this, we used the copper diffraction intensity from the Si-KS6L electrode current collector as internal standard, i.e., normalizing the silicon diffraction intensity to the copper diffraction intensity. Previous studies in the literature used nickel powder that was mixed into the silicon electrode as an internal standard in order to conduct quantitative ex-situ XRD experiments with electrodes harvested after lithiation, thereby determining the Li $_x$ Si phases that coexist with crystalline silicon (cr-Si) during the initial lithiation of crystalline silicon.²² While this is a viable approach, the in-situ XRD method used in the present study is non-destructive and allows for multiple measurements over extended charge/discharge cycling. In addition, using the copper current collector as internal standard eliminates the need for adding an internal reference, so that practically relevant electrodes can be investigated.

The quantification of the diffraction intensities was done by Rietveld refinement of the crystalline silicon and copper phases, and an exemplary Rietveld fit for a pristine Si-KS6L/Li pouch cell is given by the red line in Fig. 6, together with the difference diffraction profiles (thin black line). With the scale factors obtained from the Rietveld fit, the weight percent of the silicon (wt% cr-Si) and the copper phase (wt% Cu) can be deduced and the values are listed in Table I for the different cells and cycles each. The given errors are based on the error propagation of the refined scale factors by TOPAS. Based on the densities of copper and silicon and a loading of 2.1 mg $_{Si}$ cm $^{-2}$ and a copper foil thickness of 11 μ m, the expected weight percent of the silicon phase of the pristine cell would be 17.6 % and for the copper phase 82.4 %, this is in good agreement with the experimental values obtained from the measurement (Table I). To quantify the amount of crystalline silicon being consumed during cycling, first the ratio χ of wt% cr-Si with respect to the wt% Cu is calculated by Eq. 1 for each cycle x .

$$\chi_x = \frac{(\text{wt}\% \text{ cr-Si})_x}{(\text{wt}\% \text{ Cu})_x} \quad [1]$$

Comparison of the ratio χ_x from cycle x to the ratio χ_0 from cycle 0—determined by the weight percent of the silicon and copper phase of the pristine cell before formation—allows to calculate the relative fraction of crystalline silicon (cr-Si) being present at the respective

Table I. Weight percent of crystalline silicon phase (wt% cr-Si) and copper phase (wt% Cu) received by Rietveld refinement of in-situ XRD measurements of pouch cells cycled to 170 mV and 140 mV for 600 mAh g $_{Si}^{-1}$ and 1500 mAh g $_{Si}^{-1}$ initial capacity limit respectively. With Equation 3 the values can be converted into the relative fraction of amorphous silicon phase (a-Si) compared to the crystalline phase being present at each cycle displayed in Fig. 8b. Errors of wt% Cu and wt% cr-Si are based on the errors of the refinement of the scale factors by TOPAS, the error of a-Si was done by error propagation accordingly.

	Cycle 0	Cycle 1	Cycle 11	Cycle 21	Cycle 31	Cycle 41
600 mAh/g $_{Si}$ – 170 mV						
wt% Cu [%]	83.95 \pm 0.3	85.52 \pm 0.3	85.24 \pm 0.4	85.15 \pm 0.4	85.55 \pm 0.4	85.46 \pm 0.3
wt% cr-Si [%]	16.05 \pm 0.3	14.48 \pm 0.3	14.76 \pm 0.4	14.85 \pm 0.4	14.45 \pm 0.4	14.54 \pm 0.3
a-Si [%]	0	11.42 \pm 2.3	9.40 \pm 2.8	8.78 \pm 2.6	11.66 \pm 2.8	11.00 \pm 2.1
1500 mAh/g $_{Si}$ – 170 mV						
Cu content [%]	84.32 \pm 0.4	89.12 \pm 1.1	89.40 \pm 0.5	89.13 \pm 0.5	89.51 \pm 0.6	89.71 \pm 0.5
Si content [%]	15.68 \pm 0.4	10.88 \pm 1.1	10.60 \pm 0.5	10.87 \pm 0.5	10.49 \pm 0.6	10.29 \pm 0.5
a-Si [%]	0	34.39 \pm 7.9	36.23 \pm 3.5	34.39 \pm 3.3	36.98 \pm 4.1	38.36 \pm 3.4
600 mAh/g $_{Si}$ – 140 mV						
Cu content [%]	82.76 \pm 0.4	84.77 \pm 0.5	86.10 \pm 0.5	86.32 \pm 0.4	87.83 \pm 0.4	89.66 \pm 0.5
Si content [%]	17.24 \pm 0.4	15.23 \pm 0.5	13.90 \pm 0.5	13.68 \pm 0.4	12.17 \pm 0.4	10.33 \pm 0.5
a-Si [%]	0	13.77 \pm 3.1	22.49 \pm 3.2	23.94 \pm 2.7	33.47 \pm 2.4	44.67 \pm 3.1
1500 mAh/g $_{Si}$ – 140 mV						
Cu content [%]	85.21 \pm 0.4	89.91 \pm 0.6	91.20 \pm 0.5	93.24 \pm 0.6	96.12 \pm 0.4	/
Si content [%]	14.79 \pm 0.4	10.09 \pm 0.6	8.80 \pm 0.5	6.76 \pm 0.6	3.88 \pm 0.4	/
a-Si [%]	0	35.38 \pm 4.3	44.47 \pm 3.4	58.24 \pm 4.2	76.77 \pm 2.7	/

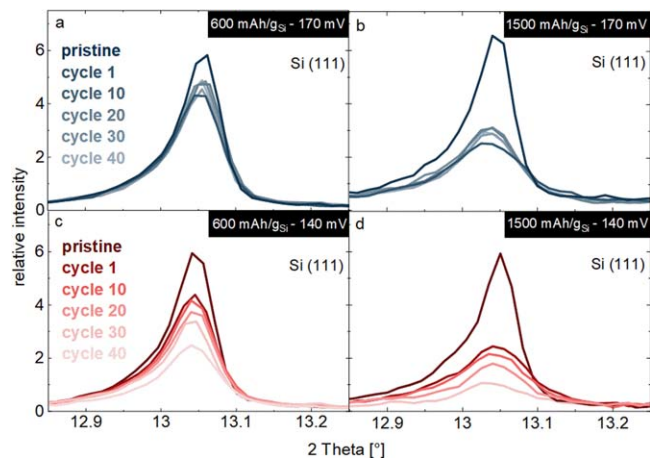


Figure 7. Magnified view of the silicon (111) reflection from in-situ XRD data of Si/Li-pouch cells cycled to a lithiation cutoff of 170 mV (a), (b) and 140 mV (c), (d) for both initial lithiation capacities of 600 mAh g_{Si}^{-1} and 1500 mAh g_{Si}^{-1} . Data were collected in the delithiated state and is shown for the pristine cell, after the first cycle and after each 10 cycles for further cycling. Intensity is normalized to the copper (111) reflection which is set to 100 counts.

cycle compared to the pristine state of the cell (Eq. 2).

$$cr-Si \equiv \frac{\chi_x}{\chi_0} = \frac{\frac{(wt\% cr - Si)_x}{(wt\% cr - Si)_0}}{\frac{(wt\% Cu)_x}{(wt\% Cu)_0}} = \frac{(wt\% cr - Si)_x}{(wt\% cr - Si)_0} * \frac{(wt\% Cu)_0}{(wt\% Cu)_x} \quad [2]$$

The relative fraction of amorphous silicon (a-Si) present at cycle x can then be calculated according to Eq. 3 and are listed in Table I.

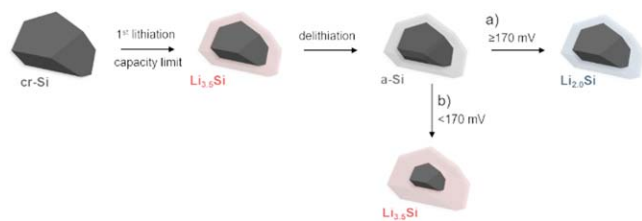
$$a-Si \equiv 1 - \frac{\chi_x}{\chi_0} = 1 - \frac{(wt\% cr - Si)_x * (wt\% Cu)_0}{(wt\% cr - Si)_0 * (wt\% Cu)_x} \quad [3]$$

(Table I) XRD spectra were taken from cells cycled to 170 mV and 140 mV each for both initial lithiation capacities of 600 mAh g_{Si}^{-1} and 1500 mAh g_{Si}^{-1} . To display the course of the silicon reflex intensity over cycling the most prominent silicon reflection (111) is shown for each cycle in Fig. 7, whereby the reflex intensity is normalized by the copper (111) reflection which is set to 100. The cycling data of these cells is shown in Figure 8a and is in good agreement with the data obtained by the T-cell setup depicted in Fig. 2. Cells cycled with a 170 mV cutoff maintain a constant horizontal capacity course over cycling whereas cells cycled with a cutoff potential of 140 mV exhibit a constant increase until a maximum capacity is reached, followed by a capacity drop. Figure 7a displays the silicon (111) reflection of the cell with an initial capacity of 600 mAh g_{Si}^{-1} and 170 mV cutoff. The pristine state exhibits the highest reflex intensity since the entire silicon is present in its crystalline phase. The silicon reflection obtained after the first cycle shows a decreased intensity for the formation of amorphous silicon phase upon lithiation to 600 mAh g_{Si}^{-1} . For continuous cycling with a cutoff of 170 mV, the measured intensity after every 10 cycles remains equal to the first cycle and does not decrease further on, thus no more additional crystalline silicon is consumed within the investigated numbers of cycles. The cell with an initial capacity of 1500 mAh g_{Si}^{-1} and a cutoff of 170 mV (Fig. 7b) shows the same behavior, even though the reduction of the silicon reflex intensity is more pronounced after the first cycle which is due to the higher initial capacity used in this case. This correlates well with the cycling data received for 170 mV where for both initial capacities 600 mAh g_{Si}^{-1} and 1500 mAh g_{Si}^{-1} the capacity does not

further increase over cycling. Next we want to look at the cells cycled to 140 mV depicted in Figs. 7c and 7d, while the reflex intensity for the first cycle of these cells is analogous the cells described above—as we would expect it since the first cycle is limited by the capacity—the course for the following cycles differ from the cells with a 170 mV cutoff. Here, we observe a significant decrease of the intensity after every 10th cycle, indicating further loss of crystalline phase during cycling. This matches well with the increasing capacity for the cells cycled with a 140 mV cutoff. The XRD data shown here correlate well with the cycling data and reveal a continuous consumption of crystalline phase for the cells cycled to 140 mV whereas cells cycled to 170 mV maintain the amount of crystalline silicon present after the initial cycle.

As described above the loss of crystalline phase during cycling can be quantified by Eq. 2 and is depicted in Figure 8b as the fraction of amorphous phase being present at the corresponding cycle for each cell. After the first lithiation we got a discharge capacity of 526 mAh g_{Si}^{-1} and 1370 mAh g_{Si}^{-1} for the cells lithiated to 600 mAh g_{Si}^{-1} (closed symbols) and 1500 mAh g_{Si}^{-1} (open symbols) respectively. Referring this to the theoretical capacity of the highest lithiated amorphous phase, which was observed by the Dahn group¹⁷ to be $Li_{3.5}Si$ (3350 mAh g_{Si}^{-1}), this would equate to 16% and 41% amorphous phase being present after the first cycle. The experimental values derived by the XRD data show a slightly lower ratio compared to the calculated values, here $11 \pm 0.2\%$ and $14 \pm 0.3\%$ of a-Si is obtained for the cells lithiated to 600 mAh g_{Si}^{-1} and $34 \pm 0.8\%$ and $35 \pm 0.4\%$ for cells lithiated to 1500 mAh g_{Si}^{-1} . Since the lithiation end potential of the first cycle is significantly lower than for consecutive cycling, capacity contribution from the graphite is more pronounced in this case. Nevertheless, correcting for the graphite capacity affects the calculated values for the expected amount of amorphous phase only marginally. Taking into consideration that the electrodes contain 25 wt% of graphite and the capacity contribution of graphite is 105 mAh g_C^{-1} at the lithiation end potential of 95 mV vs Li^+/Li for the first cycle, the lithiation degree of silicon is slightly decreased considering the graphite contribution. Therefore, the amorphous phase of the cell with 600 mAh g_{Si}^{-1} is calculated with 15% instead of 16% and the ratio of amorphous phase for the cell with 1500 mAh g_{Si}^{-1} gives 40% instead of 41%. Hence, this cannot explain the lower values obtained for the a-Si phase by the experimental data, however this does not affect the observations on the progress of the amorphous phase over cycling.

As already indicated in Fig. 7, the cells cycled to 170 mV (blue symbols) remain a constant ratio of amorphous phase once the initial lithiation cycle is conducted, however the ratio of the cells cycled to 140 mV (red symbols) constantly increases and follows almost the progress of the capacity throughout cycling. In the case of the cell with 600 mAh g_{Si}^{-1} , the ratio of a-Si increases from 14% after the first cycle to 45% after 41 cycles corresponding to a growth of 31% for the amorphous phase. While for the cell with 1500 mAh g_{Si}^{-1} the capacity only increases up to cycle 15 until the capacity drop again - this was already observed in the T-cell setup and discussed above (Fig. 2)—the amount of a-Si further increases. Here the extended capacity usage leads to electrical disconnection of particles causing the collapse of the cell, however crystalline silicon is still present and can be further consumed. At the breakdown of the cell $\sim 50\%$ amorphous phase is determined. This increases further up to 77% for cycle 31 until the sealing of the pouch cell opened due to excessive gas evolution. The cross sectional views in Fig. 5 revealed an increased surface of the silicon particles for the cells cycled to 140 mV, excessive electrolyte reduction on this surface could give an explanation for the gassing of this cell. The XRD data show that cycling silicon only to a lithiation potential of 170 mV allows to maintain the ratio of amorphous phase set in the first cycle with the capacity limit, hence decreasing the lithiation cutoff below 170 mV lead to an ongoing amorphization process during cycling causing a rapid capacity drop once the amorphous phase exceeds a critical ratio.



Scheme 2. Progress of the crystalline phase (opaque) and amorphous phase (transparent) of silicon particles upon (de)lithiation. The first lithiation is limited by the capacity forming a particle with remaining crystalline phase and a highly lithiated amorphous phase $\text{Li}_{3.5}\text{Si}$ (red). For further cycling the progress is shown for case of (a) a cutoff potential of ≥ 170 mV vs Li^+/Li , here the crystalline phase is maintained and only the lower lithiated phase $\text{Li}_{2.0}\text{Si}$ (blue) is formed. In the case of (b) the cutoff potential is limited to <170 mV vs Li^+/Li causing continuous amorphization of the crystalline phase and forming the highly lithiated $\text{Li}_{3.5}\text{Si}$.

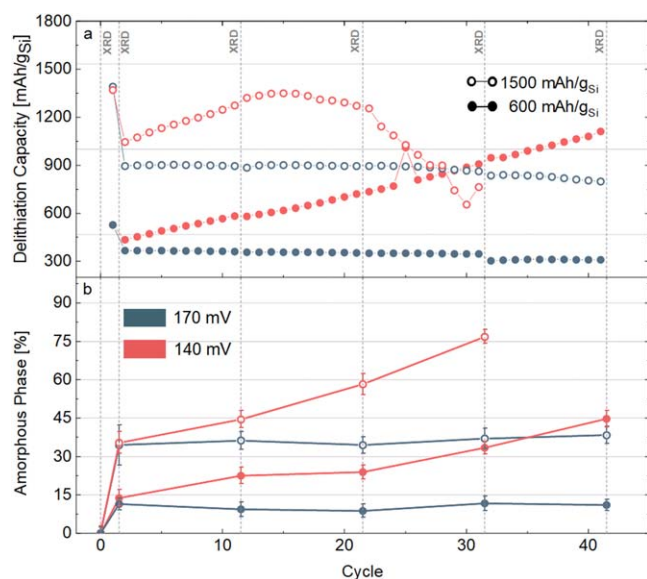


Figure 8. (a) Delithiation capacity of Si//Li pouch-cells (loading: $2.1 \text{ mg}_{\text{Si}} \text{ cm}^{-2}$; with a theoretical capacity of 7.5 mAh cm^{-2}) with a lower cutoff limit for lithiation of either 140 mV vs Li^+/Li (red) or 170 mV vs Li^+/Li (blue) for initial lithiation capacities of $600 \text{ mAh g}_{\text{Si}}^{-1}$ (closed symbols) and $1500 \text{ mAh g}_{\text{Si}}^{-1}$ (open symbols). Formation cycles were conducted by cycling at C/60 (with constant-current (CC) lithiation and delithiation), while subsequent cycling was conducted at C/30 with a CV step at the end of lithiation until a current of C/120 (C-rates are referenced to $3579 \text{ mAh g}_{\text{Si}}^{-1}$). Experiments were conducted at 25°C with 1 M LiPF_6 in FEC/DEC (2:8 v-v) and with four glassfiber separators (Whatman GD type A/E). (b) Percentage of amorphous Si phase to crystalline Si and normalized capacity of Si//Li pouch-cells with a lower cutoff limit for lithiation of 140 mV vs Li^+/Li (red) or 170 mV vs Li^+/Li (blue). Ratio of amorphous phase was derived by Rietveld-Refinement of the Si and Cu phase of in-situ X-ray diffraction measurements collected at the in-house Mo-diffractometer ($\lambda = 0.7093 \text{ \AA}$). Errors bars are min/max values and are based on the error propagation of the refinement of the scale factors by the TOPAS software.

As a result of this study Scheme 2 depicts the amorphization progress of silicon with a capacity limited material concept adapted from Obrovac et al.,³ whereby we have added the here estimated Li_xSi phase compositions. Upon first lithiation, crystalline silicon readily forms the highly lithiated $\text{Li}_{3.5}\text{Si}$ since both the lithiation reaction of cr-Si and the formation of $\text{Li}_{3.5}\text{Si}$ occur at the same potential, consecutive delithiation results in a two phase particle morphology with crystalline and amorphous silicon. The crystalline phase –preventing the particles to disintegrate– can be maintained by limiting the lithiation potential to 170 mV for further cycling, with

this only the first lithiation feature of $\text{Li}_{2.0}\text{Si}$ is observed.²⁵ However, when cycling with a cutoff below 170 mV the higher lithiated phase $\text{Li}_{3.5}\text{Si}$ is formed and ongoing consumption of remaining crystalline phase is observed causing a rapid cell failure once a critical amount of amorphous phase is reached.

Conclusions

In the present study, the amorphization process of partially lithiated silicon anodes is investigated by in-situ X-ray diffraction. First, electrochemical cycling to different lithiation cutoff potentials was analyzed and discussed. With in-situ X-ray diffraction we tracked the ratio of the amorphous and the crystalline silicon phase present during cycling, investigating different lithiation cutoff potentials. The here presented in-situ method is based on the direct measurement of the amount of the crystalline silicon phase, quantified by referencing the silicon reflex intensity to that of the copper current collector that is utilized as internal standard.

The electrochemical cycling showed a continuous capacity increase for cells cycled to a lower lithiation potential of <170 mV vs Li^+/Li . Evaluation of the dQ/dV plot of these cells showed the features of the formation of a highly lithiated $\text{Li}_{3.5}\text{Si}$ phase at these potentials.^{20,25,26} The cells cycled only to a potential of 170 mV or higher did not show the characteristic (de-)lithiation features for this highly lithiated phase and revealed a constant delithiation capacity course over the course of cycling. XRD experiments proved that cells cycled to a lithiation cutoff potential of 170 mV maintain the ratio of amorphous and crystalline phase which was set for the capacity-limited formation cycle. On the other hand, cells cycled to 140 mV reveal a constant decrease of the crystalline silicon phase, concomitant with an initial increase of the delithiation capacity over cycling, followed by a rapid capacity decrease. These results are in good agreement with the findings of a previous study by Obrovac and Krause,³ and confirm that further amorphization of the silicon particles along with an increase of the delithiation capacity will occur for cutoff potentials below 170 mV. Post mortem analysis of harvested electrodes showed severe degradation of the microscale silicon particles after 31 cycles for the cells cycled to a lithiation cutoff of 140 mV, while for the cells cycled to only 170 mV the silicon particle structure remained intact.

To enable a stable long-term cycling performance of partially lithiated microscale silicon anodes in general, it is crucial to maintain the crystalline structure of the silicon particles in order to prevent their structural disintegration. The study here demonstrates clearly that this is only accomplished by restricting the lithiation cutoff potential of the silicon anode to 170 mV or higher for consecutive cycling.

Acknowledgments

Maximilian Graf greatly acknowledges WACKER Chemie AG for its financial support. The team would like to acknowledge Christina Peters (WACKER Chemie AG) for her support with SEM sample preparation and measurement, as well as introduction on the microscope and discussion. The authors also kindly thank Benjamin Strehle (Chair of Technical Electrochemistry TUM) for support and discussions with the XRD data treatment.

ORCID

Maximilian Graf <https://orcid.org/0000-0002-2252-1216>
 Stefan Haufe <https://orcid.org/0000-0003-3025-1890>
 Hubert A. Gasteiger <https://orcid.org/0000-0001-8199-8703>

References

- U. Kasavajjula, C. Wang, and A. J. Appleby, *J. Power Sources*, **163**, 1003 (2007).
- M. N. Obrovac and V. L. Chevrier, *Chem. Rev.*, **114**, 11444 (2014).
- M. N. Obrovac and L. J. Krause, *J. Electrochem. Soc.*, **154**, A103 (2007).
- M. Wetjen, S. Solchenbach, D. Pritzl, J. Hou, V. Tileli, and H. A. Gasteiger, *J. Electrochem. Soc.*, **165**, A1503 (2018).
- J. W. Choi and D. Aurbach, *Nat. Rev. Mater.*, **1**, 16013 (2016).

6. M. Wetjen, D. Pritzl, R. Jung, S. Solchenbach, R. Ghadimi, and H. A. Gasteiger, *J. Electrochem. Soc.*, **164**, A2840 (2017).
7. X. H. Liu, L. Zhong, S. Huang, S. X. Mao, T. Zhu, and J. Y. Huang, *ACS Nano*, **6**, 1522 (2012).
8. T. Jaumann, J. Balach, M. Klose, S. Oswald, U. Langklotz, A. Michaelis, J. Eckert, and L. Giebeler, *Phys. Chem. Chem. Phys.*, **17**, 24956 (2015).
9. C. Wang, H. Wu, Z. Chen, M. T. McDowell, Y. Cui, and Z. Bao, *Nat. Chem.*, **5**, 1042 (2013).
10. N. Artrith, A. Urban, and G. Ceder, *J. Chem. Phys.*, **148**, 241711 (2018).
11. S. Choi, T. W. Kwon, A. Coskun, and J. W. Choi, *Science (80-)*, **357**, 279 (2017).
12. L. F. Cui, R. Ruffo, C. K. Chan, H. Peng, and Y. Cui, *Nano Lett.*, **9**, 491 (2009).
13. D. Jantke, R. Bernhard, E. Hanelt, T. Buhrmester, J. Pfeiffer, and S. Haufe, *J. Electrochem. Soc.*, **166**, A3881 (2019).
14. S. D. Beattie, M. J. Loveridge, M. J. Lain, S. Ferrari, B. J. Polzin, R. Bhagat, and R. Dashwood, *J. Power Sources*, **302**, 426 (2016).
15. S. Haufe, *EP3335262 B1* (2016), filed July 28, 2016 and published June 20, 2018.
16. S. Haufe, R. Bernhard, and J. Pfeiffer, *J. Electrochem. Soc.*, **168**, 080531 (2021).
17. J. Li and J. R. Dahn, *J. Electrochem. Soc.*, **154**, A156 (2007).
18. M. T. McDowell, S. W. Lee, J. T. Harris, B. A. Korgel, C. Wang, W. D. Nix, and Y. Cui, *Nano Lett.*, **13**, 758 (2013).
19. B. Strehle, T. Zünd, S. Siculo, A. Kießling, V. Baran, and H. A. Gasteiger, *In Press*.
20. K. Ogata, E. Salager, C. J. Kerr, A. E. Fraser, C. Ducati, A. J. Morris, S. Hofmann, and C. P. Grey, *Nat. Commun.*, **5**, 3217 (2014).
21. B. Key, R. Bhattacharyya, M. Morcrette, V. Seznéc, J. M. Tarascon, and C. P. Grey, *J. Am. Chem. Soc.*, **131**, 9239 (2009).
22. P. Limthongkul, Y. Il Jang, N. J. Dudney, and Y. M. Chiang, *Acta Mater.*, **51**, 1103 (2003).
23. J. Li, A. Smith, R. J. Sanderson, T. D. Hatchard, R. A. Dunlap, and J. R. Dahn, *J. Electrochem. Soc.*, **156**, A283 (2009).
24. V. L. Chevrier and J. R. Dahn, *J. Electrochem. Soc.*, **157**, A392 (2010).
25. M. J. Loveridge, M. J. Lain, I. D. Johnson, A. Roberts, S. D. Beattie, R. Dashwood, J. A. Darr, and R. Bhagat, *Sci. Rep.*, **6**, 1 (2016).
26. M. J. Loveridge, M. J. Lain, Q. Huang, C. Wan, A. J. Roberts, G. S. Pappas, and R. Bhagat, *Phys. Chem. Chem. Phys.*, **18**, 30677 (2016).
27. X. H. Liu et al., *Nat. Nanotechnol.*, **7**, 749 (2012).
28. K. N. Tu, *Appl. Phys. Lett.*, **27**, 221 (1975).
29. B. Key, M. Morcrette, J. M. Tarascon, and C. P. Grey, *J. Am. Chem. Soc.*, **133**, 503 (2011).
30. T. Yoon, C. C. Nguyen, D. M. Seo, and B. L. Lucht, *J. Electrochem. Soc.*, **162**, A2325 (2015).
31. M. Pharr, K. Zhao, X. Wang, Z. Suo, and J. J. Vlassak, *Nano Lett.*, **12**, 5039 (2012).